SWEA FM1 calibration report

Version 6.1 November, 16, 2005

Andrei Fedorov, Jean-Louis Médale, Claude Aoustin, Jean Rouzaud,

Jean-André Sauvaud

Centre d'Etude Spatiale des Rayonnements (CESR)
Toulouse, France

Content

1. Principal design and theoretical properties of the sensor

The SWEA analyzer optics is shown in Figure 1. The properties of the analyzer calculated analytically are as follows:

1. The K factor which is the ratio of the energy per charge of the electrons *E/Q* [eV/<electron charge>] to the potential of the inner hemisphere *Uan* [V] :

$$K = \frac{E/Q}{Uan} = \frac{R1}{2.(R2 - R1)} = 6.7$$

2. The aperture area:

$$S = \frac{2}{3}.(R2 - R1).2\theta.R1 = 0.45 \text{ cm}^2$$

3. The normalized velocity space volume (expressed as the product of the energy resolution by the width of the elevation acceptance angle:

$$\left\langle \frac{\Delta E}{E} \Delta\alpha \right\rangle = \frac{1}{2}\left(\frac{R2 - R1}{R1} \right)^2 \csc^3\left(\frac{90 - \sigma}{2} \right)\left(\frac{7}{8} + \cos\left(\frac{90 - \sigma}{2} \right) \right) = 0.017 \text{ rad.eV/eV}$$

4. The total geometrical factor for the 360° field of view:

$$GF = 4\pi.\frac{2}{3}.\left\langle \frac{\Delta E}{E}.\Delta\alpha \right\rangle.(R2 - R1).R1.\theta = 0.033 \text{ cm}^2.\text{sr.eV/eV}$$

Numerical simulations of the sensor give results quite close to the analytical one, as displayed in Table 1 (see Annex 4 for a detailed description of the simulation results):

Elevation,	K	ΔE/E	GF, cm^2.sr.eV/eV
-54.9	6.38	0.137	3.23E-02
-48.3	6.35	0.181	4.26E-02
-40.3	6.33	0.180	4.09E-02
-21.8	6.39	0.187	3.72E-02
1.1	6.36	0.176	3.32E-02
19.4	6.36	0.170	3.86E-02
41.6	6.27	0.173	3.88E-02
52.8	6.24	0.143	2.80E-02
61.1	6.19	0.119	1.18E-02

Table 1 : *Summary table of the results of the numerical simulations of SWEA*

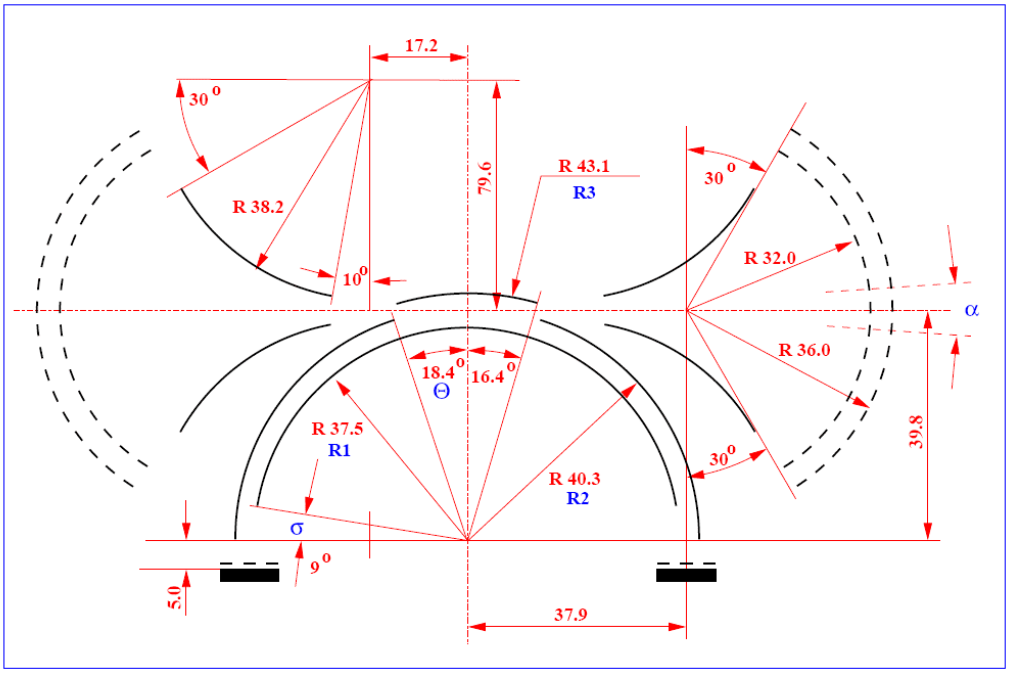

Figure 1: *Electrostatic optics of the SWEA sensor. The main dimensions used to calculate the analyzer properties are marked in blue. α is the elevation angle acceptance range.*

2. Electrical setup and calibration constants

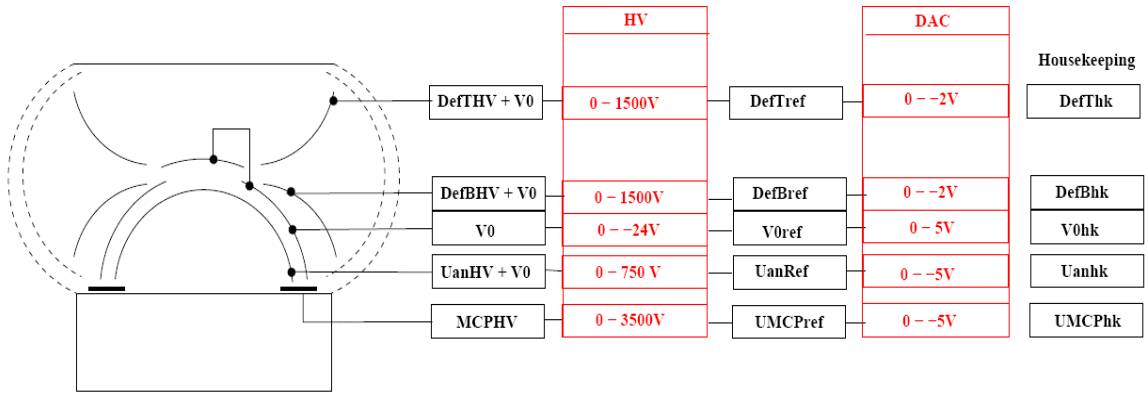

Figure 2: *Electrical block diagram of the SWEA calibration setup. The DAC is located outside of the vacuum chamber. The DAC resolution is 0.lmV. All housekeeping values are recorded with accuracy of 0.1 mV.*

The electrical setup is shown in Figure 2. The correspondence of reference, high voltage, and housekeeping values is as follows:

$V0$ [V] = -5.000×10^{-3} $V0ref$ [mV] - 1.366 × 10^{-3}

$V0$ [V] = -5.001×10^{-3} $V0hk$ [mV] + 1.796 × 10^{-3}

$UanHV$ [V] = -1.503×10^{-1} $UanRef$ [mV] + 2.222 × 10^{-2} + $V0$

$UanHV$ [V] = 0.1689 $Uanhk$ [mV] - 0.1236

$UdefTHV$ [V] = -0.7467 $UdefTref$ [mV] + 0.2545 + $V0$

$UdefTHV$ [V] = 0.3311 $UdefThk$ [mV] + 0.1835

$UdefBHV$ [V] = -0.7540 $UdefBref$ [mV] + 0.0249 + $V0$

$UdefBHV$ [V] = 0.3349 $UdefBhk$ [mV] - 0.0125

$MCPHV$ [V] = -0.687 $UMCPref$ [mV] + 18.22

$MCPHV$ [V] = 1.003 $UMCPhk$ [mV] - 2.25

(Note that these calibration values are valid for $T = 20°C$).

3. MCP gain and dead-time

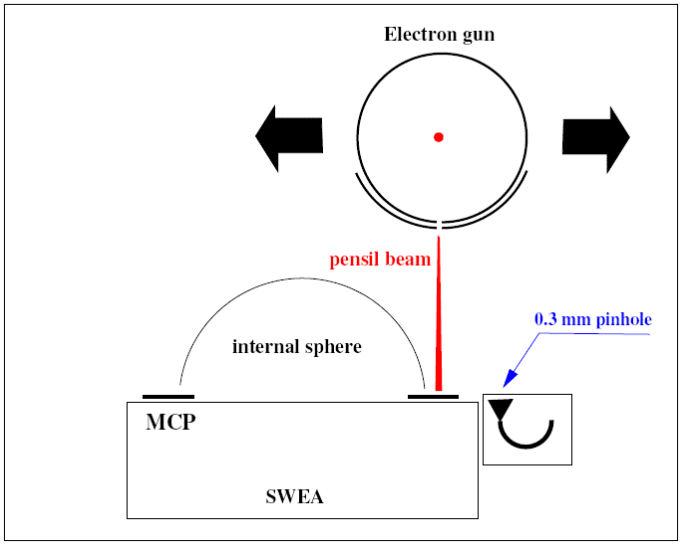

Figure 3: *Setup for MCP characterization. Pin-holes of 0.5mm diameter are located at 76.6mm firom the center of the sensor, in the middle of each azimuthal sector. The gun has been movedalong Y and Z to illuminate each sector successively. The beam intensity is controlled by the total current collected on the cylinder surrounding the gun. A CEM is also used to control the beam. The beam dynamics is* 10^3.

The setup for the characterization of the MCP is shown in Figure 3. The electron beam is narrow in the *Y* direction and has a non-uniform (even multi-peaked) distribution in the *Z*

direction. It is worth to note that the shape of the distribution is independent of the total electron current (see Annex l for details). The gun can be moved along *Y* and *Z* to illuminate each pinhole. The total electron current of the beam is *Jbeam* = *Jmeas* × 0.0127. Here *Jmeas* is the current emitted by the gun and collected on the surrounding cylinder. The beam profile at the MCP level is given in Figure 4.

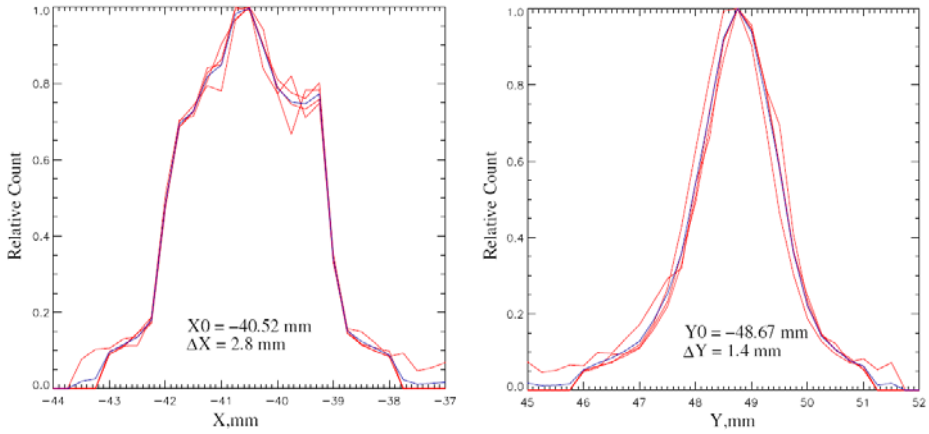

Figure 4: *Y (left panel) and Z (right panel) normalized profiles of the electron beam*

MCP gain

The count rate of each MCP sector versus *MCPhk* value is shown in Figure 5. Subsequent SWEA calibration has been made with *MCPhk* = 2750 mV, corresponding to *MCPHV* = 2756 *V*.

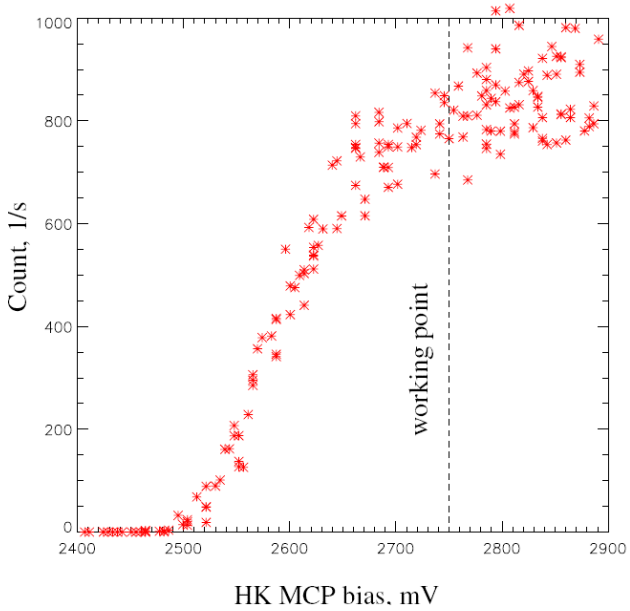

Figure 5: *Count rate versus MCPHV[V] for selected MCP sectors. The vertical dashed line shows the working point for the subsequent calibrations.*

Dead-time

The spatial distribution of the electron current produced by the gun does not change when the total flux is increasing. We use this gun property to measure the MCP dead-time. The method to measure the deadtime is the following:

1. The beam current is changed from 4.10^3 s^{-1} up to 8.10^4 s^{-1} (i.e electrons/s).

2. For each beam current the MCP count rate is recorded. The count rate profile was normalized assuming that the dead-time of the MCP is negligible at low count rates.

4. Find the flux versus the measured count rate of a single channel is shown in Figure 6.

In a simple dead-time model the count rate is:

$$\Phi = \frac{C}{1 - C.\tau} \qquad (2)$$

Here C is the measured count rate, τ is the dead-time of a single channel and Φ is the real count rate. The solid line in Figure 6 corresponds to a dead-time of 200 ms.

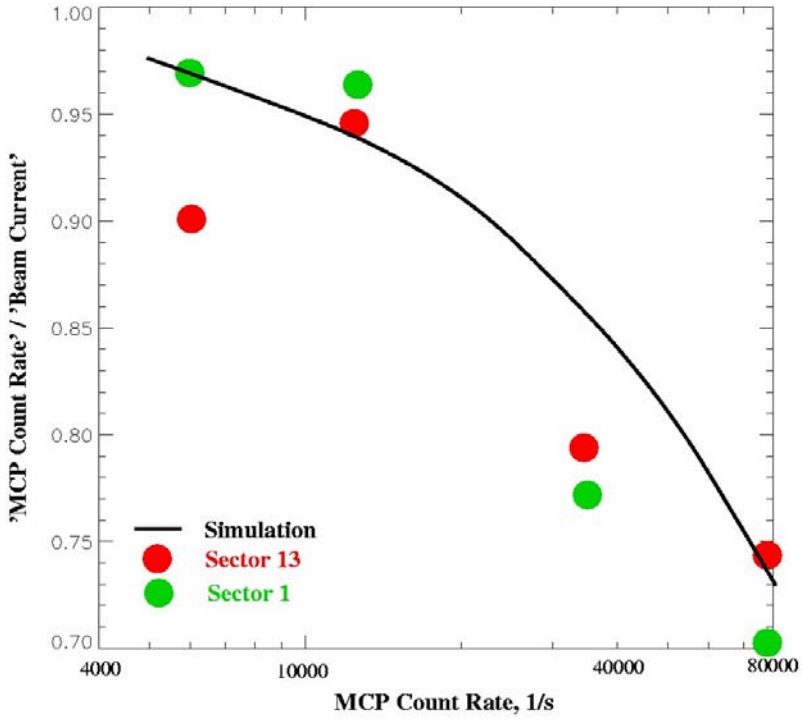

Figure 6: *MCP normalized count rate versus the incident total flux of electrons. The black curve correspond to* τ *= 200 ms*

Conclusions:

Minimal MCPHV:	2756 V
Single MCP channel dead-time:	200 ms

4. Calibration setup. Mechanical coordinate system. Electron beam properties.

Here we give only a brief introduction to the SWEA calibration mechanical setups. Annex 3 furnishes detailed explanations. The general setup is shown in Figure 7. The sensor can be rotated around the Y axis and the gun can be displaced along the Z and Y axis. Actually we used two different sensor positions: 1) as shown in Figure 7 (left), called "positive" setup; 2) upside-down position when SWEA axis is anti-parallel to Z, called "negative" setup (not shown). "Positive" setup is used to investigate the upper hemisphere of the SWEA field-of-view, and "negative" setup is used to investigate the lower hemisphere of SWEA.

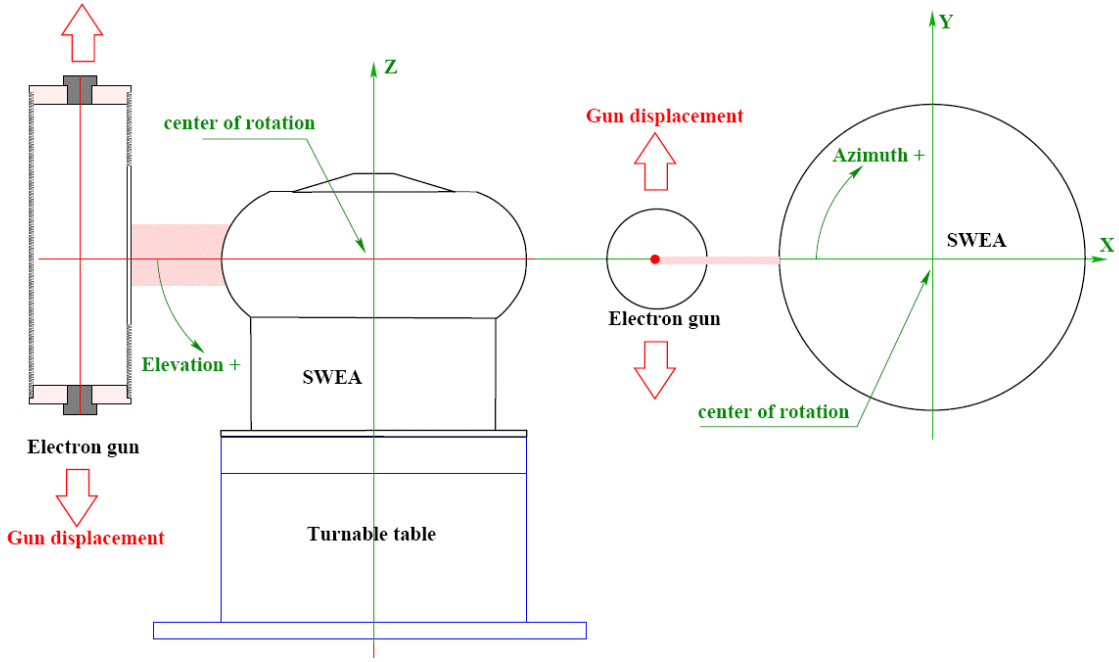

Figure 7: *Calibration setup and coordinate system for SWEA tests, (see Annex 3).*

Electron beam

The properties of the electron gun are described in Annex 1 (for SWEA FM1) and Annex 3. Its main properties are given below:

1. The beam is narrow in the Y direction. Its thickness can be considered as negligible.

2. The gun produces a parallel 2D electron beam in the XZ plane. The beam is not uniform in the Z direction. Superposing the beam for several Z positions of the gun allows obtaining a nearly uniform beam.

3. The stability of the electron gun is about 10%. The gun current *Jmeas* is read for each SWEA count reading.

Mechanical terms

Mechanical terms are introduced in Figures 7 and 8 as follows:

Θ_M - mechanical rotation of the instrument around Y (elevation)
Φ- mechanical azimuth equal to the beam azimuth
Y_{GUN} - gun shift from the XZ plane
Z_{GUN} - vertical gun position.
Θ - beam elevation (see Figure 8)
Ω - latitude where the electron beam crosses the external grid of SWEA

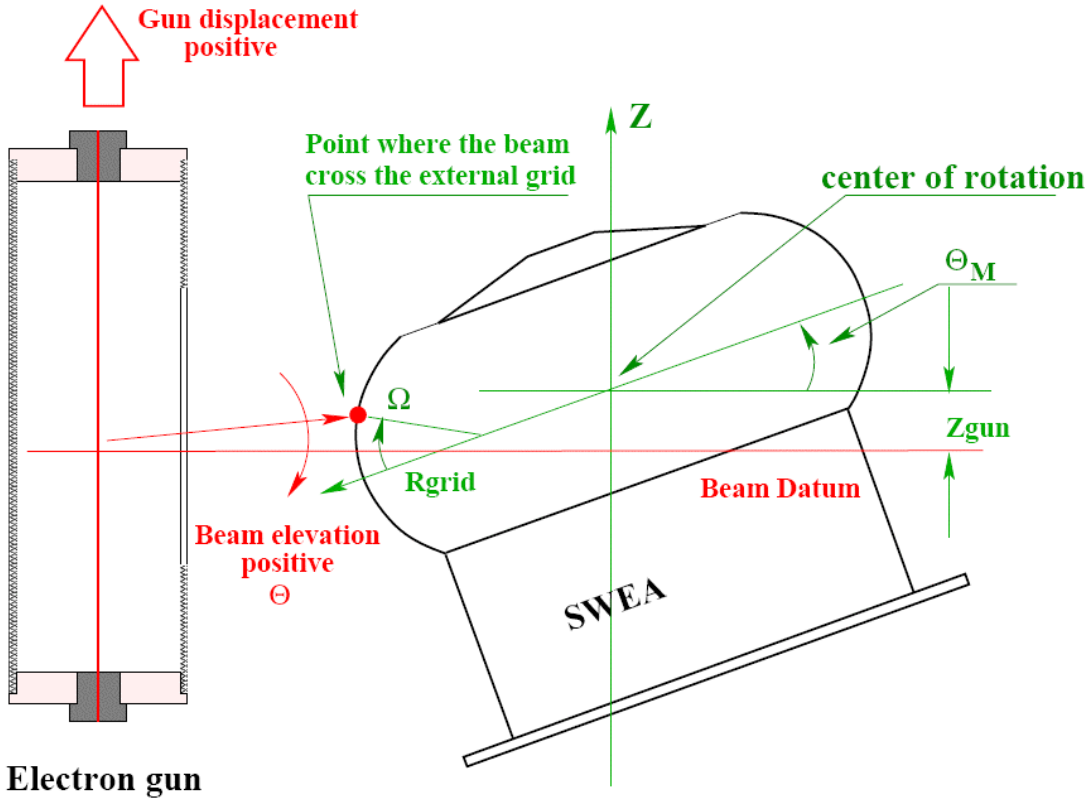

Figure 8: *Calibration scheme in the XZ plane; valid for the "negative" as well as for the "positive" setups.* Θ *is the beam elevation.* Θ_M *is the mechanical rotation angle of the sensor. The beam crosses the exterior grid of the sensor at the point defined by* Ω (the *centre of this angle is the centre of the grid curvature).*

5. Electrostatic terms, measurement scheme, and instrument response

Electrostatic terms

The electron trajectories inside the analyser are defined by the ratio

$$K = (E/Q)/Uan \qquad (0)$$

Here *E* is the electron energy in eV, *Q* is the electron charge, (= 1), and *Uan* is the analyzer voltage. The other value defining the electron trajectories in the deflector part of the sensor is:

$$D = (UdefTHV - UdefBHV)/(E/Q) \qquad (1)$$

Here *UdefTHV* and *UdefBHV* are the voltages applied to the top and the bottom electrodes of the deflector (see section 2). Later we will use *Udef = UdefTHV - UdefBHV*.

Measurement scheme and *E -Θ* response

Count rate versus *K* and *D* is shown in Figure 9. This distribution corresponds to a fixed beam direction and to a fixed electron energy. The electrodes voltages are swept. In the reality we need to obtain the response of the instrument when *Udef = const* and *Uan = const* (or equivalently *D·K = const)* for various *E* and Θ. For a fixed Θ this corresponds to a sweep along one red trajectory in Figure 9. Note that *K* corresponds to *E* in any case. Shifting the entire distribution along *D* is equivalent to change Θ. Hence we can replace the mechanical Θ variations by changing the red trajectory in the *D — K* space. For *K = K0* (centre of the energy response) the transformation from *D* to Θ will be:

$$(\Theta-\Theta 0) = -(d\Theta/dD).(D-D0) \qquad (2)$$

dΘ/dD is obtained from the calibration (see Annex 3 for details). D0 is the center of the D response. Thus having the D-K response, we can transform it into the E-Θ response (see examples in section 6)

Geometrical factor of the sensor

For a given Φ and a given (*D·K)*, let us define G_{lin} *[cm². rad. eV/eV]* as the "azimuthal density" of the geometrical factor of the sensor, i.e. the integral of the effective aperture over *E/E0* and over the elevation angle.

$$G_{lin} = \{\Sigma\Sigma\ CountY(\Theta_i,K_j).(\Delta K/K0).\Delta\Theta\}/P \qquad (3)$$

Here *P* is the electron current linear density [$cm^{-1}\cdot s^{-1}$](see section 3), Δ*K* is the *K* step of the measure-ment, and ΔΘ is the reconstructed virtual Θ acceptance step. *CountY* = Σ*Count.ΔY is* the integral over the Y_{GUN} sweep (see the next section).

The final geometrical factor of one sector, *GF*, is the integral *oî* G_{lin} over the sector azimuthal width.

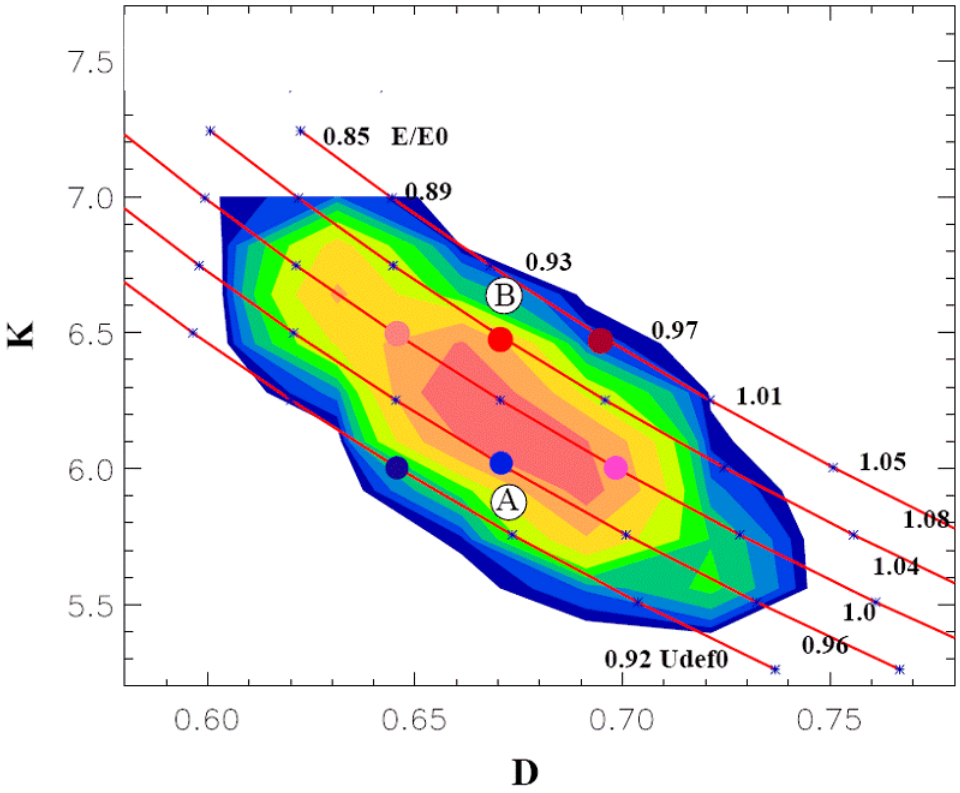

Figure 9: *Count distribution for Θ_M = 50°. Red lines show the Uan = const and Udef = const paths corresponding to different Udef. The corresponding E/E0 values are shown on the upper side. The Udef/Udef0 ratio is given near each red line.*

6. Master plan of the calibrations

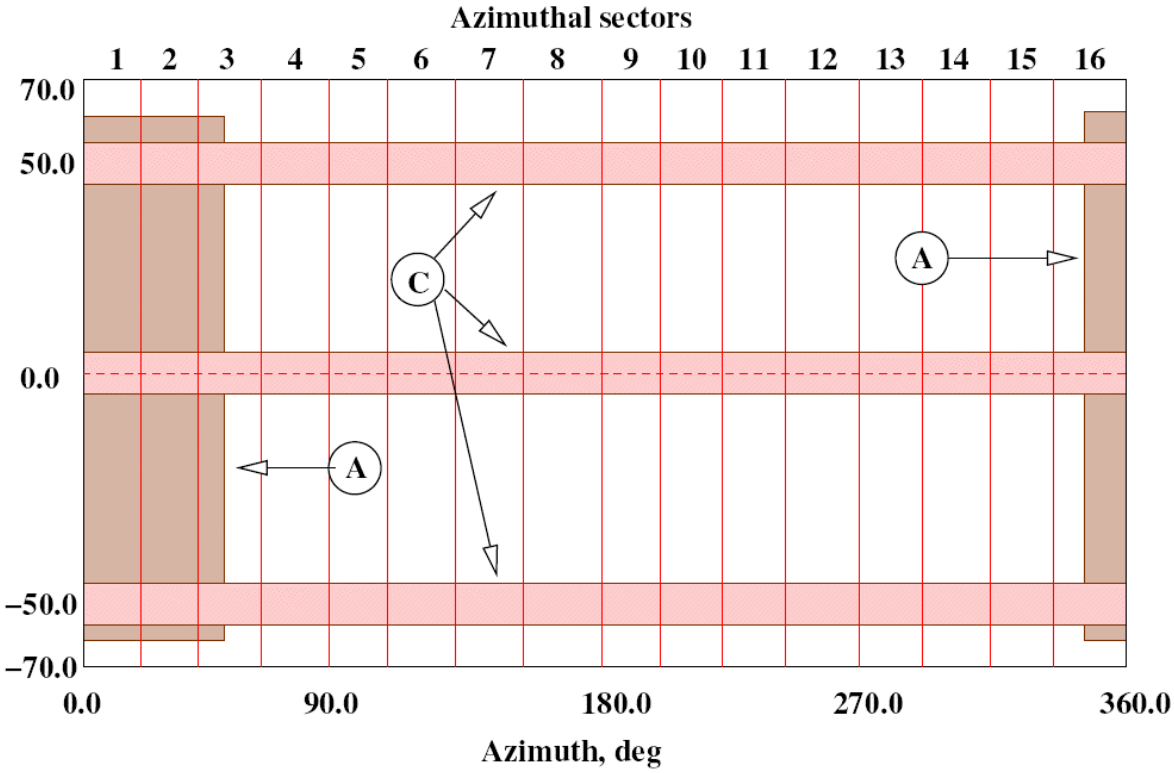

Figure 10: *Calibration master plan. Parts of the angular range of the instrument have been surveyed by different measurements modes (**A** and **C**). See text for details.*

A number of technical measurements were performed (see Annex 3) to adjust the calibration regimes to the instrument. Thus the *K*, Θ, and Φ steps and ranges have been chosen. Also the Z_{GUN} origin and the gun sweeping ranges and steps have been defined after the first test measurements (see Annex 3 for details). It is worth to note here that a change of the beam vertical position results in a change of Θ_M. Since the *Z* width of the beam is restricted, we have to keep the center of the beam distribution always at the center of the sensor aperture. To perform this, an appropriate function has been obtained from the technical measurements (see Annex 3):

For "positive" setup the Z_{GUN} compensation is:

$$Z0[\text{mm}] = 0.946 - 0.588\ \Theta_M + 0.001 \times 10^{-6} \times \Theta_M^2 \qquad (4)$$

For “negative setup”, this value is:

$$Z0[\text{mm}] = -1.87 - 0.5196 \times \Theta_M - 0.0019.10^{-6} \times \Theta_M^2 \qquad (5)$$

The function dΘ/dD has been measured versus Θ:

$$d\Theta/dD[\text{deg}] = 79.26 - 10.88 \times D \qquad (6)$$

After several adjustments the following measurements have been made (see Figure 10):

A – Measurements of the elevation response using 10° elevation steps between –60° and +60°of Θ_M range. These measurements have been done for a limited azimuthal range corresponding to the 1st azimuthal sector.

C - Measurements over the entire azimuthal range with a 3° resolution, for three fixed Θ_M values. Since for positive and negative elevations different SWEA setups are used, zero mechanical elevation has been tested two times.

In each measurement mode the measurement sequence was:

1. For the given value of Θ_M do:
2. Calculate D0 using equation 8.
3. Set the $Z0_{GUN}$ gun position according to equation 4 or 5
4. For each Y_{GUN} gun position from-16.0 mm to +16.0 mm with a 4 mm step do:
5. For a set of Z_{GUN} gun positions from $Z0_{GUN}$ = 8 mm to $Z0_{GUN}$ = 7 mm with a 2.5 mm step do:
6. Measure the count rate at 13 *K* points in the interval 5.0 to 7.7 for each of 11*D* values in the interval D0 - 0.2 to D0 + 0.2
7. For the "positive" setup sum all *D* - *K* distributions taken at individual *Z* positions of the gun.
8. Integrate (trapeze method) all *D* - *K* distributions obtained for different Y_{GUN} positions (see section 7).
9. Convert each *D* - *K* distribution to the Θ - *K* one.

The complete measurement and data processing scheme is given in Annex 3.

7. Data processing and examples of sensor responses

For each individual (fixed Φ) Θ-*K* spectrum, G_{lin} has been calculated. Then, using this integral value, we can transform the Θ-*K* spectrum to the effective aperture function of Θ and *K*.

Figure 11, 12,13, and 14 show examples of the measured and simulated sensor aperture as a function of Θ and *K* measured for a fixed Φ corresponding to the middle of an anode sector.

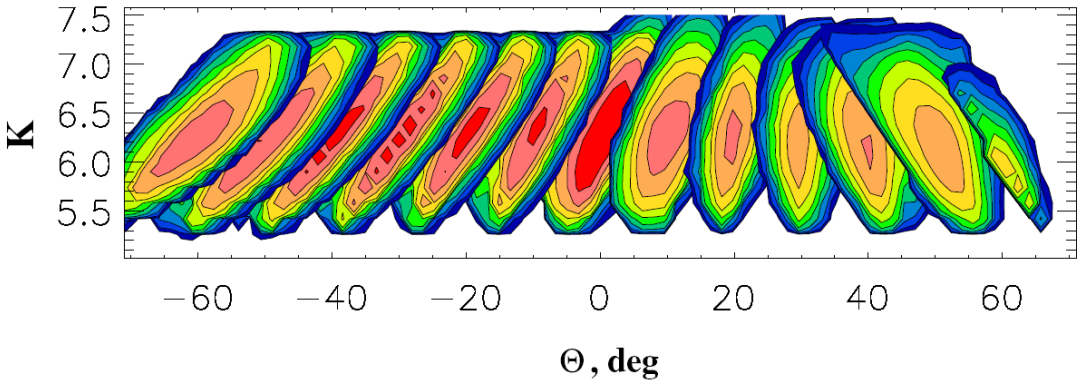

Figure 11: *Summary of the 2D plots of SWEA effective aperture as a function of Θ and K for different D values. These measurements correspond to mode* ***A*** *(see Figure 10).*

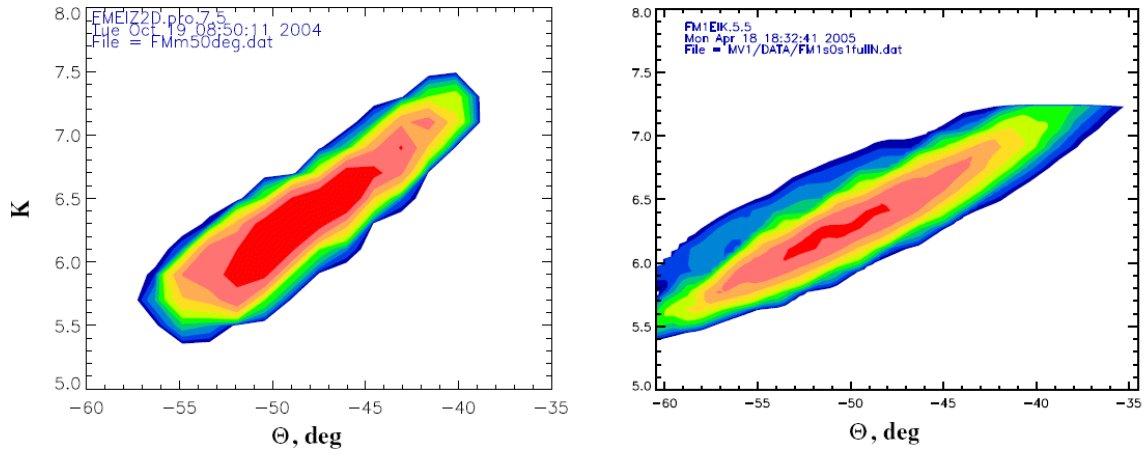

Figure 12: *2D plots of SWEA effective aperture as a function of Θ and K for D= -0.59. Contours are spaced by √2. Left panel illustrate the simulation results, and right panel shows the measurements.*

The following Figure 15, shows examples of the *K*, Θ responses of the instrument in mode A. These profiles are shown for measurements and simulations for a given azimuth Φ = –32°. The measured profiles are fairly consistent with the simulation results shown by dashed curves (see Annex 4).

Conclusions:

1. The *K*-Θ response of the sensor is very variable with *D* (i.e. elevation angle);
2. The $D \Rightarrow \Theta$ reconstruction method is adequate.
3. The SWEA measured properties are generally consistent with simulation results.

The next two sections describe the complete set of the sensor properties versus elevation angle.

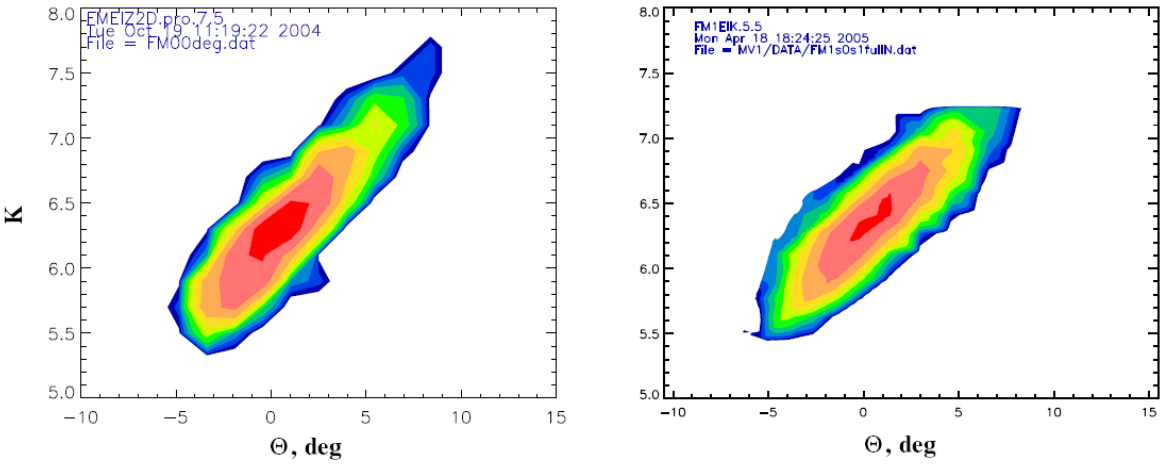

Figure 13: *Same as Figure* 12 *but for D0* =0.03.

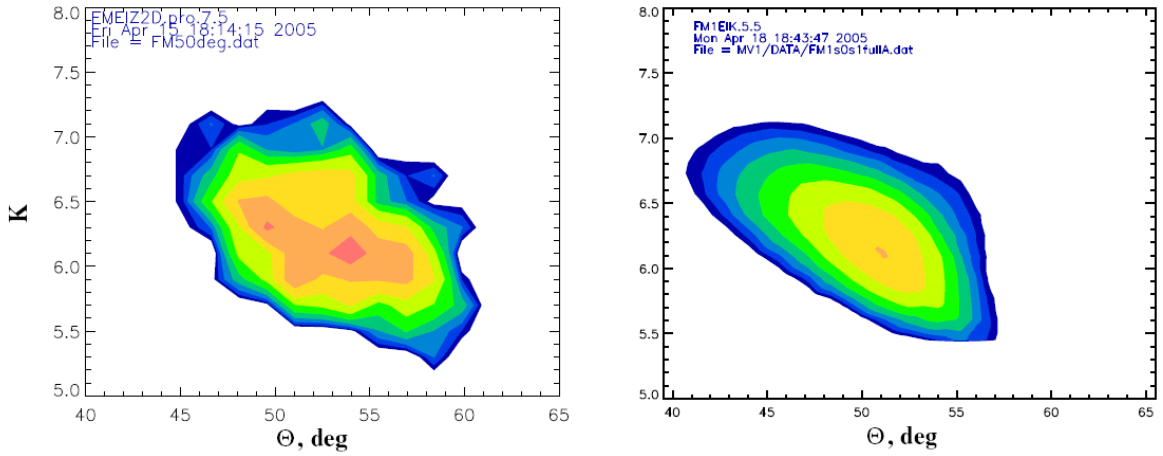

Figure 14: *Same as Figure* 12 *but for D0* = 0.71.

8. D-Elevation properties of the sensor

D - Θ properties have been obtained in mode **A** (see Figure 10). In all cases, measurements have been made for an azimuthal angle corresponding to the maximum count of the 1st azimuthal sector. The main results of these measurements are shown in Figure 16. Here,

each profile corresponds to a specific D0 value. A number giving the line number in the resulting Table 2 marks each profile.

Each profile is the "effective aperture" *S* (see Annex 3) integrated over the energy response of the sensor for a given Θ_M (note that the azimuthal angle is constant). Thin curves show the Gaussian fit of the instrument responses. This fit simplifies the calculation of the G*lin* values. Note the strong asymmetry of $\Delta\Theta$ for positive and negative elevations.

Figure 17 show the simulation results to be compared with the measurements.

A relative degradation of the experimental effective aperture versus the theoretical one is apparent for high elevations. This could be explained by the entrance grid interference and grid support interference (see Figure 23).

The main limitation of the instrument is clearly apparent: the range of possible elevation angles is limited to: -60° to +60°.

Another important result is the *D* versus Θ_μ function which allows to calculate the needed electrode voltages to reach a given elevation angle. This profile is shown in Figure 18. There is a good agreement between theoretical and experimental values. Finally the D-Θ functions are given below:

$$\Theta_\mu[\text{deg}] = -2.9 + 78.3 \times D0 - 1.22 \times D0^2 \quad (7)$$

$$D0 = 3.7 \times 10^{-2} + 1.28 \times 10^{-2} \times \Theta_\mu[\text{deg}] + 2.54 \times 10^{-6} \times \Theta_\mu[\text{deg}]^2 \quad (8)$$

These functions are practically linear in the valid range of the elevation angles.

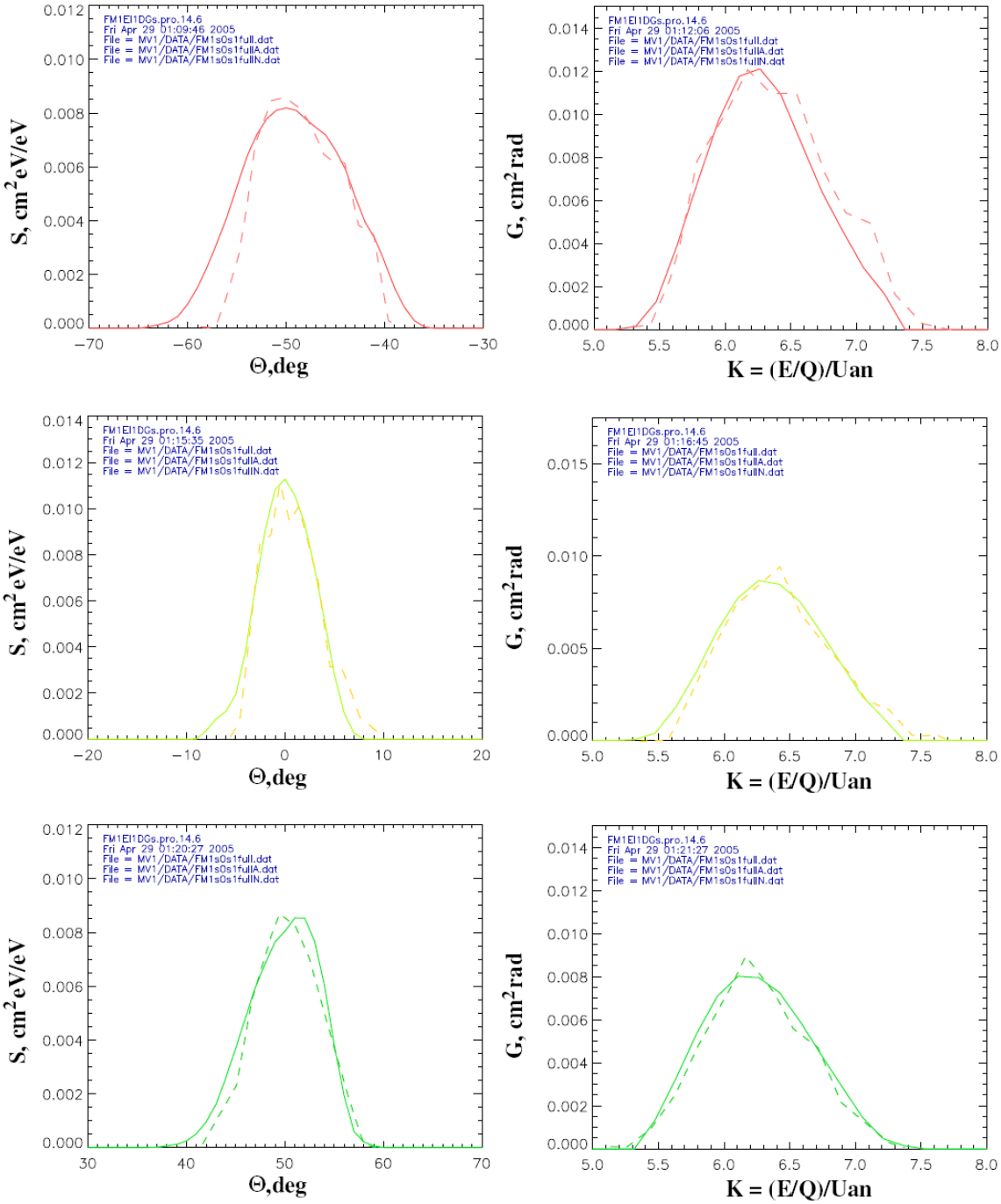

Figure 15: *Top row of two panels : examples of the sensor responses for azimuths corresponding to the center of the first azimuthal sector, for D = -0.59. Left panel in this row show the Θ properties, and the right panel show K properties. Dashed curves gives the results of numerical simulations. Middle and low rows of panels show the same for D = 0.03 and D = 0.71 correspondingly.*

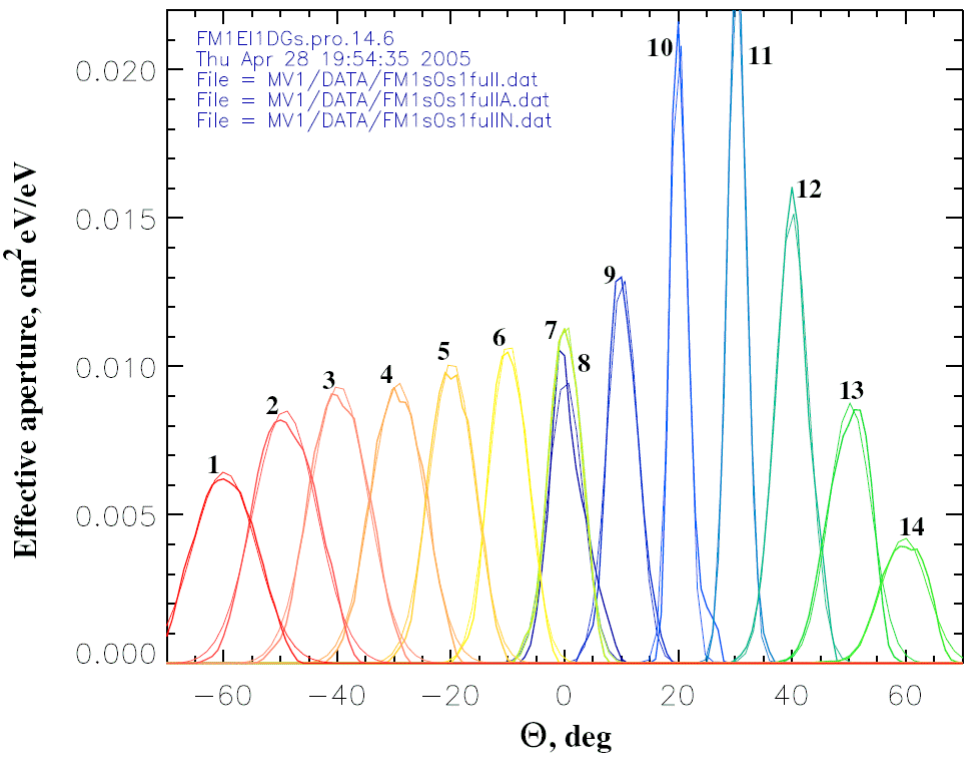

Figure 16: *Effective aperture versus the Θ angle for several D0 values, measured for the "negative" sensor setup (#8-14) and for positive setup (#1-7). Thin lines show the Gaussian fit of the profiles. Details of each profile including the exact position of the medium elevation angle and the corresponding* D0 *can be found in Table 2. The numbers on the curves in the Figure correspond to the line numbering of Table 2*

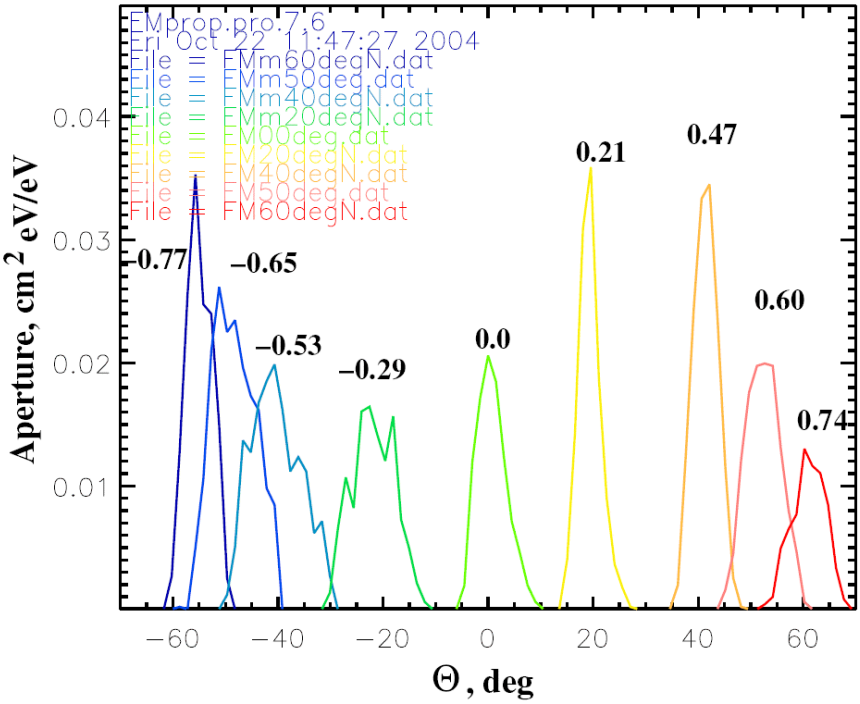

Figure 17: *Same as Figure 16 but for simulation results.*

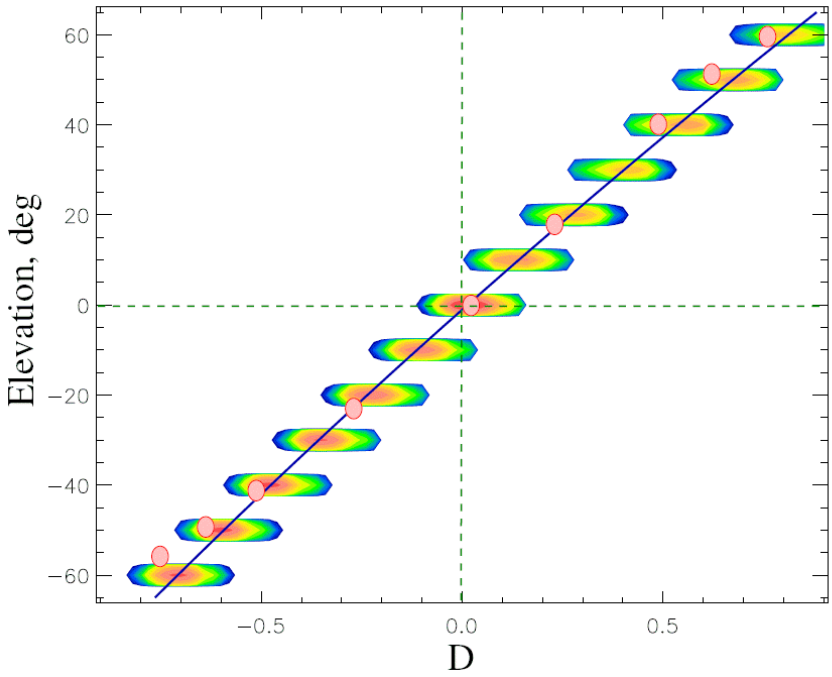

Figure 18: Θ_M *versus* D0. *Blue asterisks show experimental points. The solid line corresponds to the best fit of the experimental points (see text). The red circles indicate the result of the sensor simulation (see Annex 4).*

9. Sensor properties versus elevation angle for a given azimuthal direction.

This section gives the variation of the main properties of the sensor versus the elevation angle for constant azimuths. The geometrical factor density (Glin) versus elevation is shown in Figure 19. It worth to note that for the data presented in Figures 17 – 22, there is no difference between Θ_M and Θ. Measurements are consistent with the simulation results if the efficiency of the sensor (grids, MCP, etc.) is 0.25. The geometrical factor can be described as:

$$\text{Glin}\ [\text{cm}^2.\ \text{rad.}\ \text{eV/eV}] = 1.48 \times 10^{-3} - 2.31 \times 10^{-6} \times \Theta[\text{deg}] + 3.67 \times 10^{-7} \times \Theta[\text{deg}]^2 \quad (9)$$

Figure 20 shows the variation of the K0 factor versus Θ. Note the good agreement with simulation data. K0 can be expressed as:

$$K = 6.28 - 7.29 \times 10^{-5} \times \Theta[\text{deg}] + 4.58 \times 10^{-6} \times \Theta[\text{deg}]^2 \quad (10)$$

The $\Delta E/E$ value is slightly less than the predicted one. It ois expressed as:

$$\Delta E/E = 0.167 + 2.95 \times 10^{-6} \times \Theta[\text{deg}] \quad (11)$$

Finally the width of the elevation response $\Delta\Theta$ versus Θ is shown in Figure 22. Note that $\Delta E/E$ and $\Delta\Theta$ are calculated as integral under the curve divided by the curve maximum. A Gaussian best fit has been used to calculate the integral and the maximum of the response.

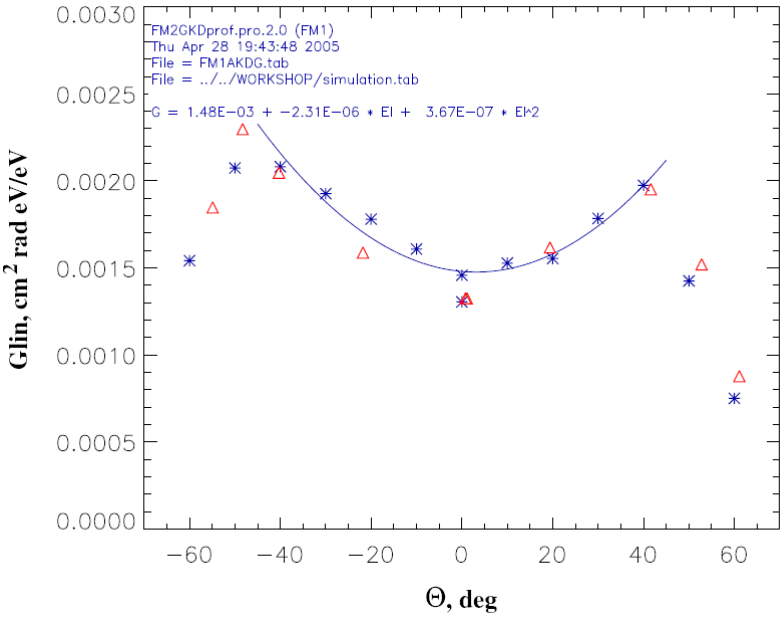

Figure 19: *G_{lin} profile versus elevation angle measured for a fixed azimuthal angle corresponding to the middle of the first azimuthal sector. Blue asterisks are the experimental values and red triangles show results of the numerical simulation taken with a factor 0.25 (cf. Annex 4)*

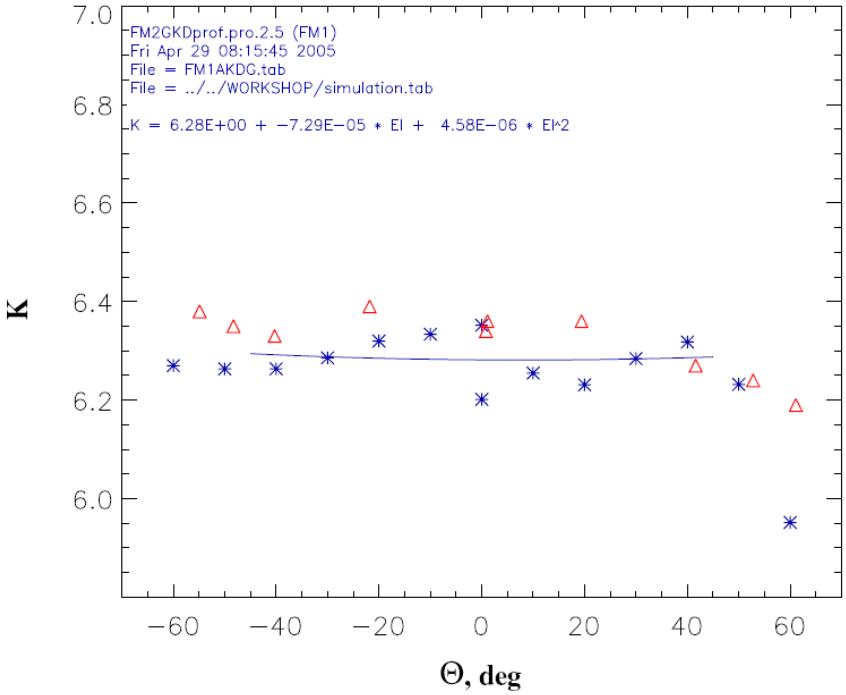

Figure 20 : *K versus elevation measured for an azimuth corresponding to the center of the 1st azimuthal sector.*

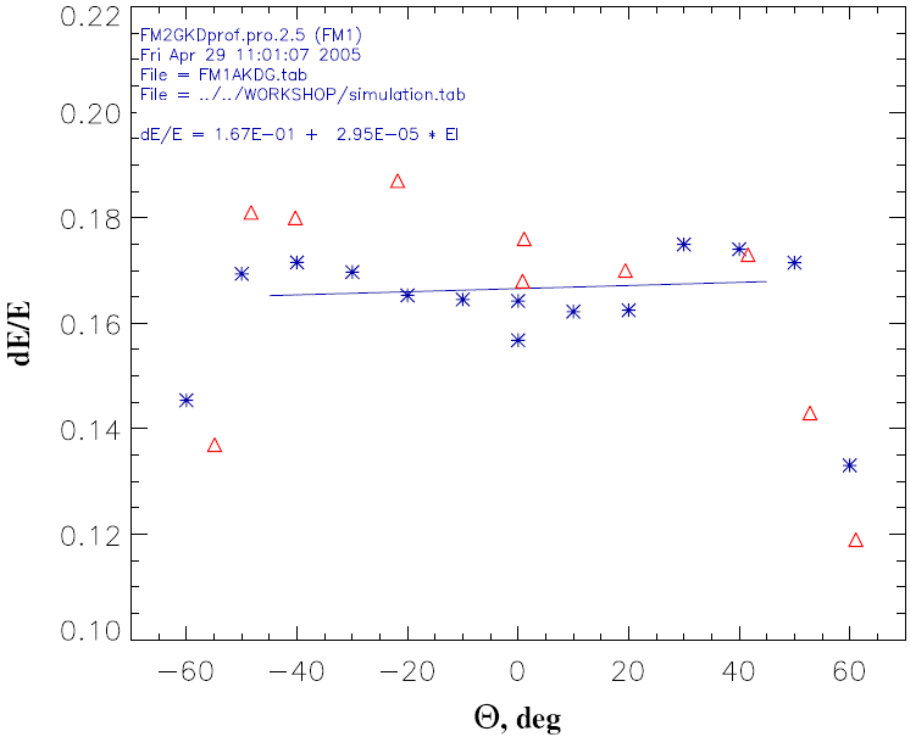

Figure 21 *: ΔE/E versus elevation angle. Conditions are the same as for Figure 20*

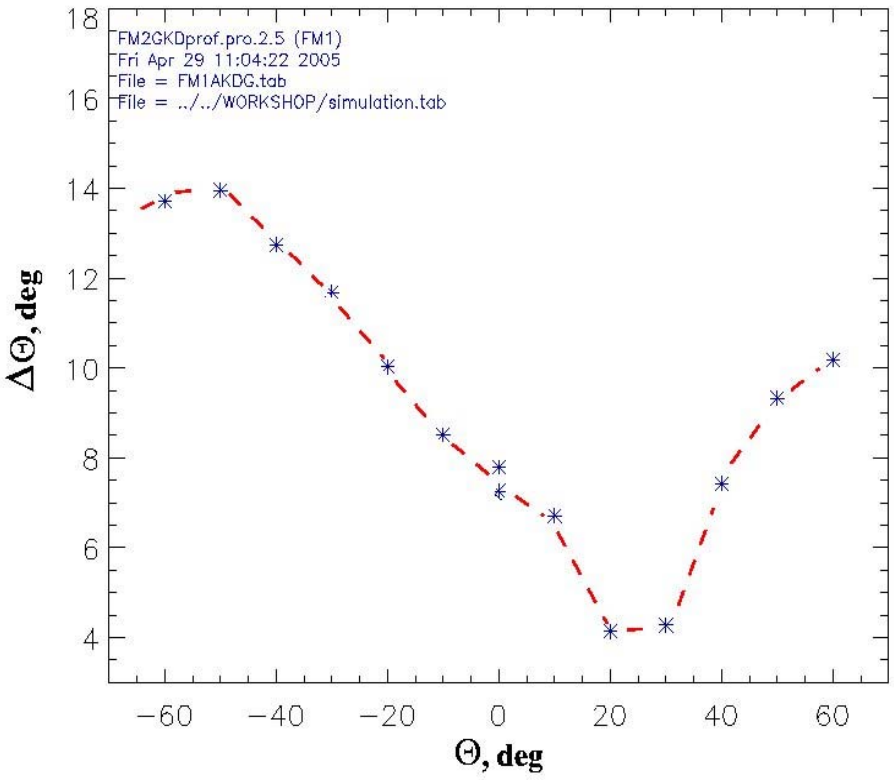

Figure 22: *Elevation response versus elevation angle. Conditions are the same as for Figure 20*

N	Θ,deg	D	ΔΘ,deg	K	ΔE/E	$G_{lin} cm^2$ radeV/eV
1	-60.0	-0.703	13.7	6 .27	0. 0.145	1.54E-03
2	-50.0	-0.587	14.0	6 .26	0. 0.169	2.07E-03
3	-40.0	-0.470	12.7	6 .26	0. 0.172	2.08E-03
4	-30.0	-0.340	11.7	6 .29	0. 0.170	1.93E-03
5	-20.0	-0.220	10.0	6 .32	0. 0.165	1.78E-03
6	-10.0	-0.095	8.5	6 .33	0. 0.165	1.61E-03
7	0.0	0.047	7.8	6 .20	0. 0.157	1.30E-03
8	0.0	0.027	7.3	6 .35	0. 0.164	1.46E-03
9	10.0	0.165	6.7	6 .25	0. 0.162	1.53E-03
10	20.0	0.299	4.1	6 .23	0. 0.162	1.55E-03
11	30.0	0.424	4.3	6 .28	0. 0.175	1.78E-03
12	40.0	0.549	7.4	6 .32	0. 0.174	1.97E-03
13	50.0	0.705	9.3	6 .23	0. 0.171	1.43E-03
14	60.0	0.830	10.2	5 .95	0. 0.133	7.50E-04

Table 2: *Summary table of SWEA properties for a specific azimuthal angle corresponding to the center of the first azimuthal sector*

10. Sensor properties as a function of the azimuthal angle for several elevations.

The effect of the grid support on the sensor transmission has been evaluated. The comparison of such a sector Φ-response with numerical simulations is shown in Figure 23.The grid support reduces the geometrical factor of the sector and changes the profile of the acceptance. This is not important for high elevations (right panel). Thus this sector azimuthal response never has a flat part and its maximum is shifted from the support location.

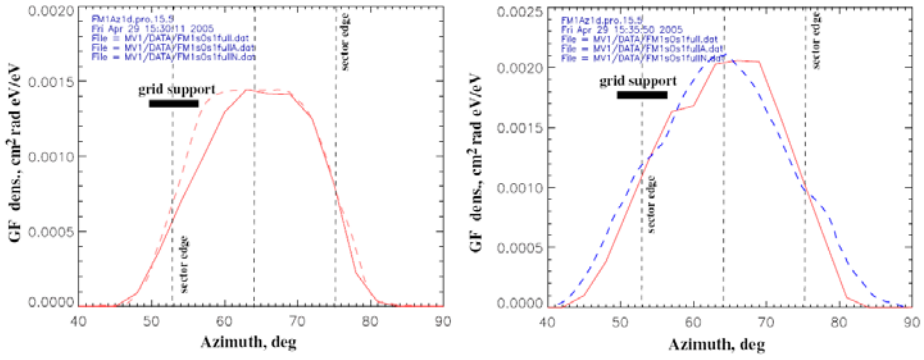

Figure 23: *Comparison of simulated (dashed) and measured (solid) Glin for* Θ_M *= 0° (left panel) and* Θ_M *= -50° (right panel). In both cases the simulated Glin has been plotted with a reduction factor of 0.25*

As mentioned in section 6, the azimuthal properties of the sensor for several specified elevation angles was measured (mode **C**). For each setup, namely "negative" and "positive", such a measurement has been done for elevations of 50° and 0°. Thus the measurements without deflection for two different setups can be compared (and for two different electron guns).

Complete test results are shown in Figures 24, 25, 26, and in Tables 3, 4, 5, and 6.

Glin [cm^2.rad . eV/eV] versus the azimuth angle is shown in Figure 24 for four different elevations. The integration of Glin over the azimuth for each azimuthal sector gives the full geometrical factor of each sector. These geometrical factors are given in the Tables 3, 4, 5 and 6. The other figures show the variations of *K* and *D* versus azimuth. These variations can be described by the following expressions:

Θ = -50.0°: ("négative")

$$K = 6.27 - 2.46 \times 10^{-2} \times \sin(\Phi) + 8.23 \times 10^{-2} \times \cos(\Phi) \quad (13)$$

$$D = -0.60 + 3.47 \times 10^{-4} \times \sin(\Phi) + 8.44 \times 10^{-3} \times \cos(\Phi) \quad (14)$$

Θ = 0° ("négative"):

$$K = 6.26 + 1.17 \times 10^{-2} \times \sin(\Phi) + 6.8 \times 10^{-2} \times \cos(\Phi) \quad (15)$$

$$D = 0.035 - 5.22 \times 10^{-3} \times \sin(\Phi) + 7.15 \times 10^{-5} \times \cos(\Phi) \quad (16)$$

Θ = 0° ("positive"):

$$K = 6.24 + 4.69 \times 10^{-2} \times \sin(\Phi) + 5.16 \times 10^{-2} \times \cos(\Phi) \quad (17)$$

$$D = 0.042 + 6.1 \times 10^{-4} \times \sin(\Phi) + 4.9 \times 10^{-3} \times \cos(\Phi) \quad (18)$$

Θ= 50.0° ("positive"):

$$K = 6.23 + 5.21 \times 10^{-2} \times \sin(\Phi) + 5.28 \times 10^{-2} \times \cos(\Phi) \quad (19)$$

$$D = 0.697 - 1.12 \times 10^{-2} \times \sin(\Phi) - 6.0 \times 10^{-4} \times \cos(\Phi) \quad (20)$$

Sector	Azimuth, deg	K	D	GF *cm^2 sr eV/eV*
1	64.5	6.30	-0.595	7.76E-04
2	84.9	6.26	-0.592	7.42E-04
3	107.4	6.21	-0.600	7.24E-04
4	129.7	6.21	-0.604	5.81E-04
5	153.7	6.19	-0.603	7.74E-04
6	165.4	6.19	-0 608	
7	-160 6	6.21	-0 599	
8	-141.9	6.23	-0.600	7.11E-04
9	-116.1	6.25	-0.607	6.72E-04
10	-97.4	6.28	-0.602	8.48E-04
11	-72.6	6.32	-0.595	8.62E-04
12	-51.7	6.33	-0.589	7.75E-04
13	-26.2	6.36	-0.585	8.20E-04
14	-7.9	6.36	-0.589	5.33E-004
15	18.6	6.33	-0.589	8.27E-04
16	39.0	6.32	-0.592	7.23E-04

Table3: *Azimuthal properties of SWEA for Θ_M = -50.0° ("négative" setup). The geometrical factor is given in cm^2.sr.eV/eV.*

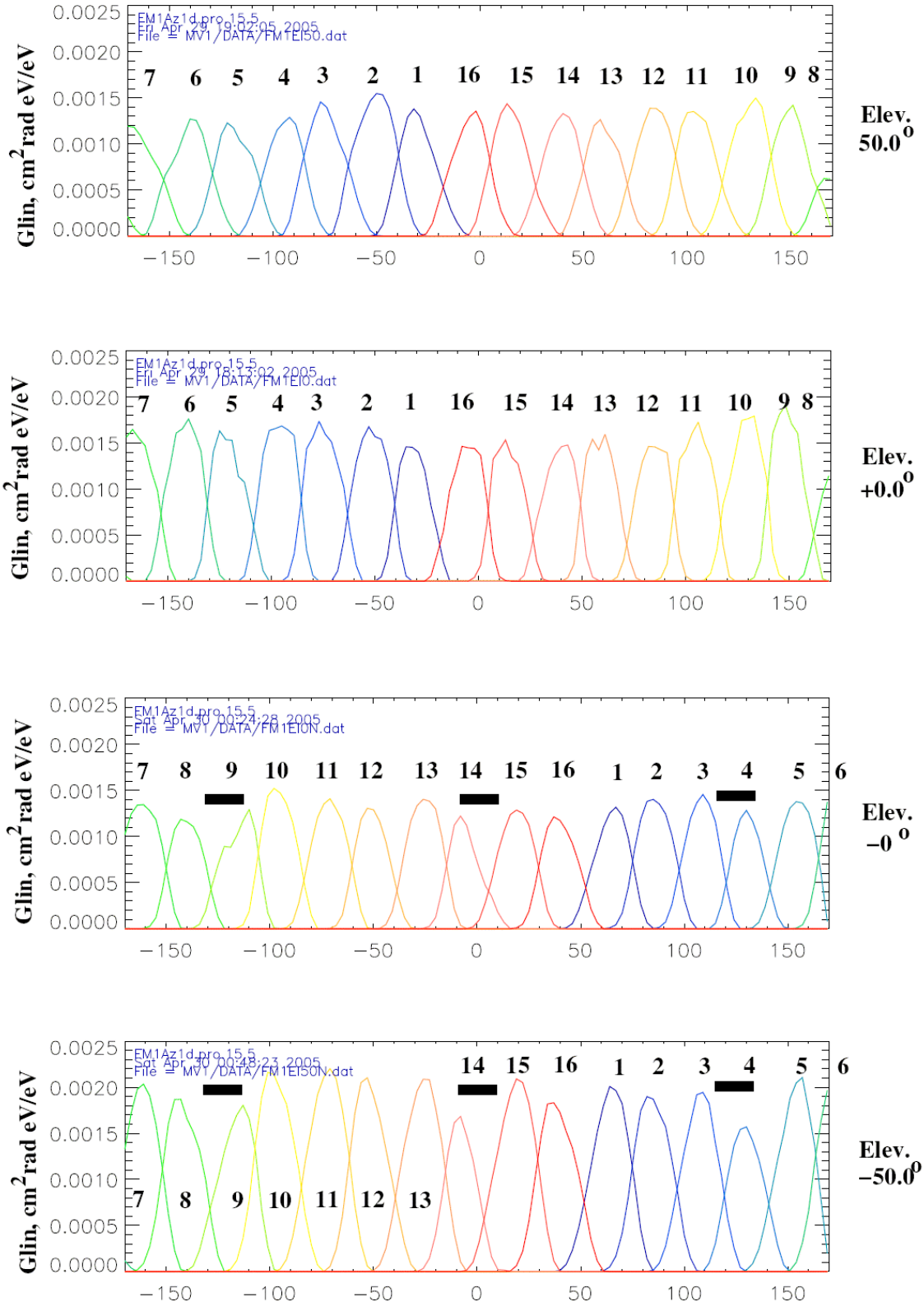

Figure 24: *G_{lin} versus Φ for four different elevation angles. The two bottom panels correspond to the "negative" mechanical setup and the two top panels correspond to the "positive" mechanical setup. Numbers on the curves indicate the azimuthal sector number.*

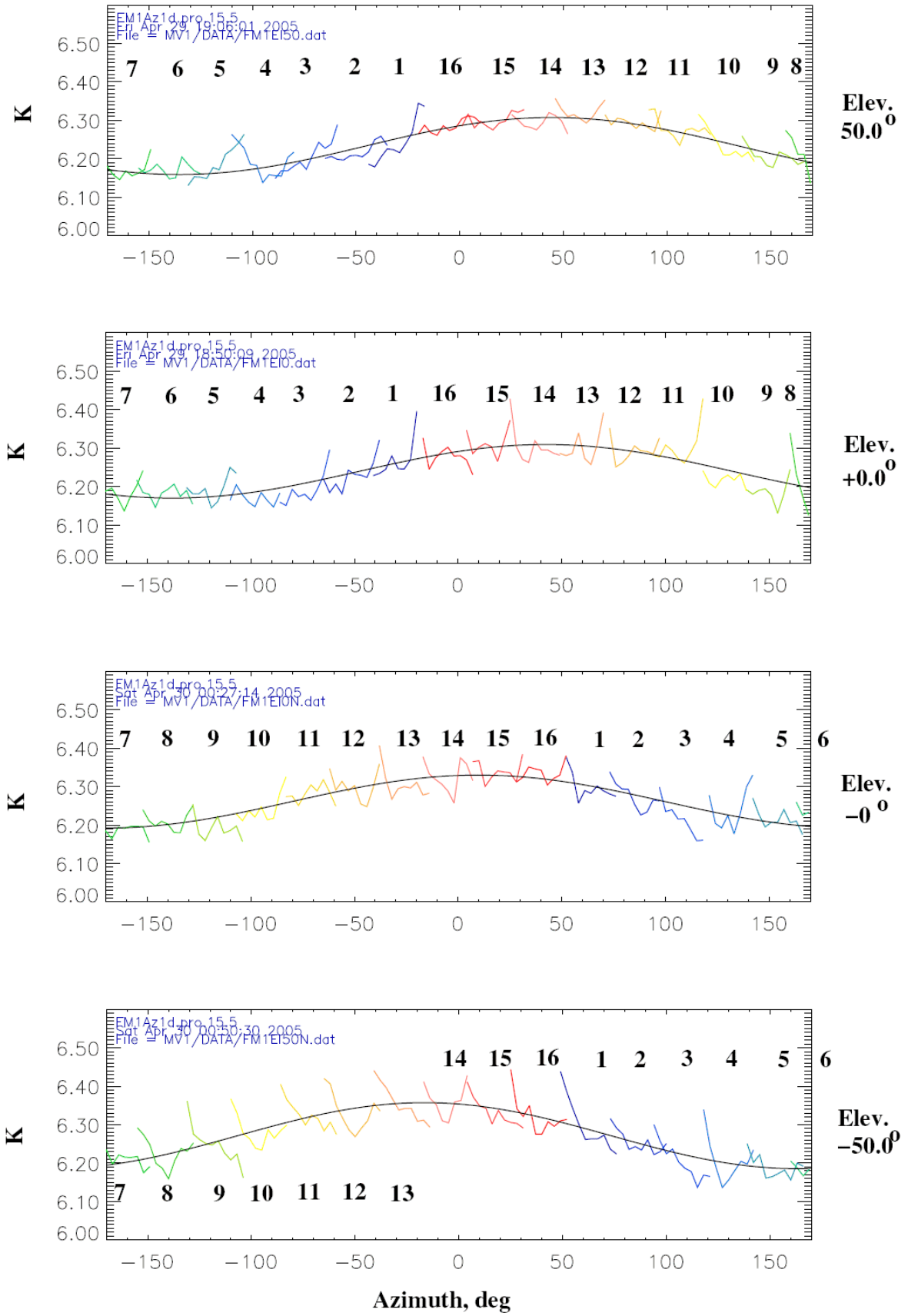

Figure 25: *K versus Φ for four different elevation angles. Layout is the same as in Figure 24*

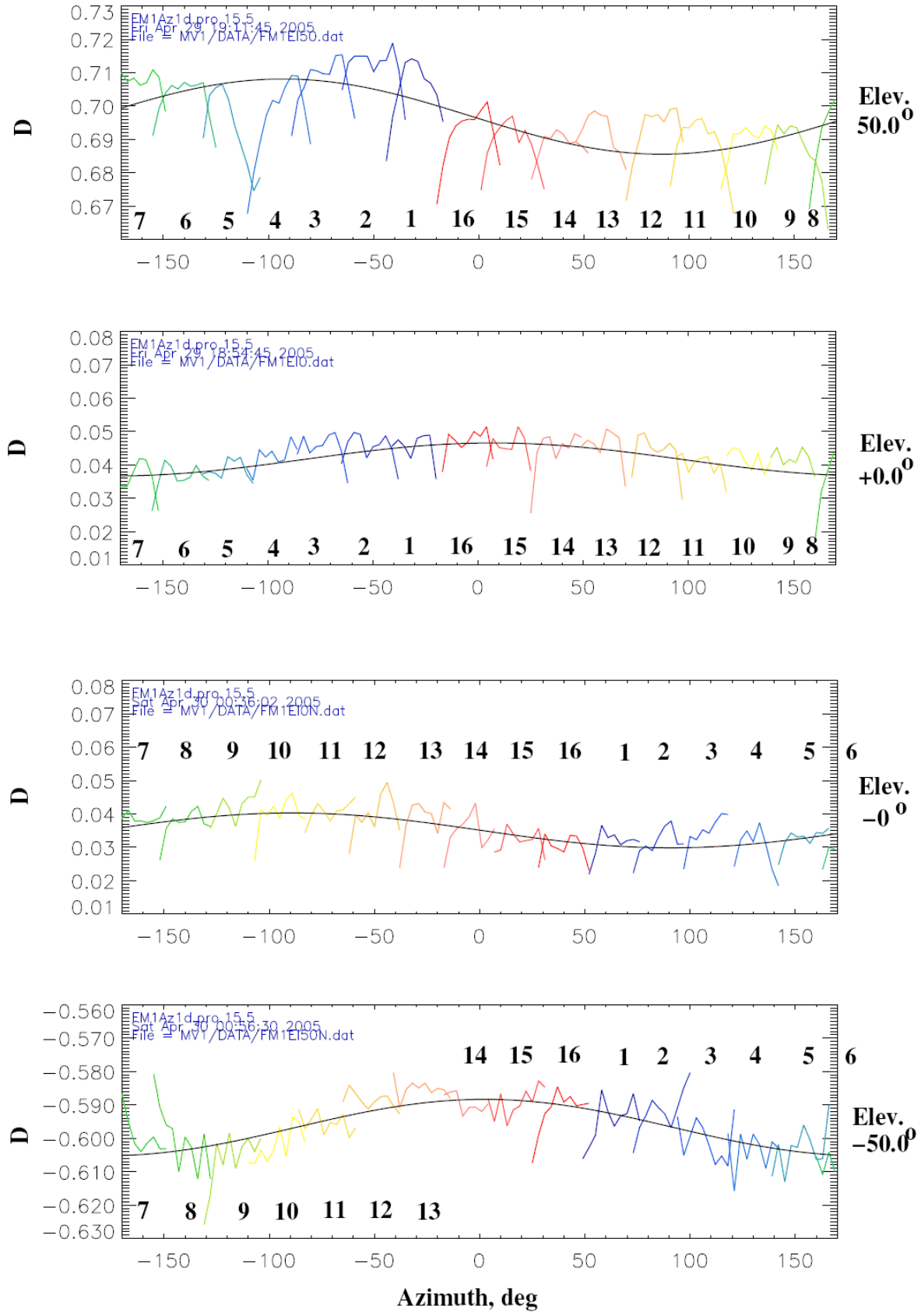

Figure 26: *D versus Φ for four different elevation angles. Layout is the same as in Figure 24*

Sector	Azimuth, deg	K	D	GF cm^2 sr eV/eV
1	65.1	6.30	0.031	4.73E-04
2	85.9	6.27	0.031	5.35E-04
3	108.3	6.21	0.034	5.04E-04
4	130.4	6.24	0.029	4.02E-04
5	154.2	6.22	0.033	5.20E-04
6	167.0(?)	6.24	0.028	
7	-160.4(?)	6.18	0.039	
8	-140.1	6.21	0.037	4.22E-04
9	-115.0	6.19	0.042	4.43E-04
10	-95.6	6.24	0.040	5.38E-04
11	-71.4	6.28	0.041	5.18E-04
12	-50.6	6.30	0.040	4.47E-04
13	-25.6	6.31	0.038	5.22E-04
14	-5.6	6.33	0.034	3.87E-04
15	18.9	6.34	0.032	4.88E-04
16	40.1	6.33	0.030	4.44E-04

Table 4: *Same as Table 3 but for $\Theta = 0°$ ("négative" setup)*

Sector	Azimuth, deg	K	D	GF cm^2 sr eV/eV
1	-31.3	6.27	0.045	4.92E-04
2	-51.6	6.23	0.045	6.15E-04
3	-75.2	6.19	0.045	6.27E-04
4	-96.3	6.17	0.042	6.39E-04
5	-120.8	6.19	0.038	5.60E-04
6	-141.6	6.18	0.036	6.30E-04
7	-162.6(?)	6.19	0.036	
8		6.22	0.033	
9	149.0	6.19	0.042	6.23E-04
10	129.1	6.22	0.042	6.29E-04
11	105.0	6.30	0.040	5.93E-04
12	84.3	6.29	0.043	5.29E-04
13	59.0	6.30	0.046	5.34E-04
14	39.1	6.30	0.044	5.23E-04
15	14.2	6.31	0.045	5.04E-04
16	-5.7	6.28	0.046	5.25E-04

Table 5: *Same as Table 3 but for $\Theta = 0°$ ("positive" setup).*

Sector	Azimuth, deg	K	D	GF cm^2 *sr eV/eV*
1	-30.2	6.24	0.704	3.31E-04
2	-50.7	6.22	0.711	4.21E-04
3	-74.7	6.20	0.707	3.70E-04
4	-94.4	6.19	0.695	3.21E-04
5	-118.6	6.19	0.693	3.11E-04
6	-139.8	6.17	0.701	3.27E-04
7	-161 7	6 17	0.707	
8		6 21	0.686	
9	150.1	6.21	0.685	3.44E-04
10	129.8	6.24	0.689	3.82E-04
11	104.7	6.28	0.687	3.53E-04
12	84.1	6.30	0.692	3.64E-04
13	59.4	6.32	0.692	3.05E-04
14	39.4	6.29	0.688	3.39E-04
15	14.7	6.30	0.688	3.50E-04
16	-5.0	6.29	0.691	3.31E-04

Table 6: *Same as Table 3 but for Θ = 50.0° ("positive" setup).*